SYNTHESIS AND CHARACTERISATION

OF RAMAN NANOTAGS

FOR MOLECULAR

DETECTION

by

JAMES O NYAGILO

Presented to the Faculty of the Graduate School of

The University of Texas at Arlington in Partial Fulfillment

of the Requirements

for the Degree of

MASTER OF SCIENCE IN BIOENGINEERING

THE UNIVERSITY OF TEXAS AT ARLINGTON

December 2008

ACKNOWLEDGEMENTS

ABSTRACT

SYNTHESIS AND CHARACTERISATION

OF RAMAN NANOTAGS

FOR MOLECULAR

DETECTION

James O Nyagilo, MS

The University of Texas at Arlington, 2008

Supervising Professor: Digant Dave'

The realization that most diseases are preceded or accompanied by changes in the genetic and cellular level of an organism has increased with the need for imaging modalities, with the sensitivity and specificity, to quantitatively detect biomolecules at those levels. Specifically there has been a need for the development of a modality that has the ability to detect multiple biomolecules from a single sample in order to increase accuracy of molecular diagnosis and allow for early detection of terminal diseases.

Surface enhanced Raman spectroscopy provides potential for such a modality. The distinct spectrum of each Raman active molecule serves as a molecular "fingerprint" enabling it to be clearly distinguished from other Raman spectra. Although Raman signals are fundamentally much weaker than signals produced by most other modalities, they can be enhanced by the use of electron rich metallic nanoparticles such as gold nanoparticles by 14 – 15 orders of magnitude. Additionally, gold's reported biocompatibility and its well documented

use in dentistry and in the treatment of Rheumatoid Arthritis give it a unique advantage over other labeling materials.

In this thesis, the synthesis and characterization of gold nanoparticles for optimum Surface Enhanced Raman Scattering within the optical window is described. Using these nanoparticles, five of nanotags were developed distinguished from each other by the different reporter molecules on them. These nanotags are shown to remain stable under harsh conditions and have a great potential for detection of multi-cellular expression *in vivo* and *in vitro*.

TABLE OF CONTENTS

vi

LIST OF ILLUSTRATIONS

LIST OF TABLES

CHAPTER 1

MODERN MODALITIES OF MOLECULAR DETECTION

1.1 <u>Background</u>

Many pathological conditions are preceded or accompanied with changes on a cellular level. Cancer in particular is considered to occur due to mutations within the cells that affect regulation of cellular events [1]. Examples include bone morphogenetic protein 7, a signaling molecule associated with bone metastasis which has been implicated in breast cancer pathogenesis [2] and reports that evolving stages of lung cancer are accompanied with changes in genetic and protein expression levels within the cells [1]. These reports underline the need for modalities that can be used, at a cellular level, to detect diseases. One of the driving motivations for the development of such modalities is the importance of early detection in allowing for more effective therapy and therefore mitigating the effects and of cancer and other diseases that are considered to be terminal.

A wide range of modalities for the detection of cellular expression exist in the market. They include: ellipsometry, spectroscopy (luminescence, phosphorescence, fluorescence, Raman), interferometry and surface plasmon resonance [3]. In the current practice, the most widely used methods for detection of molecular quantities involve labeling of those quantities. Three of the most common methods are Radioactivity, fluorescence and chemiluminiscence [4]. These modalities have been instrumental in the detection of various aliments including Human Immunodeficiency Virus (HIV) [5] and detection of tumors [6, 7] with current research increasingly focused in the molecular detection of metastasis in cancer [8, 9].

However despite these developments, "technological platforms that provide reliable, rapid, quantitative, low-cost and multichannel identification of biomarkers such as genes and proteins are *de facto* the rate limiting steps for the clinical deployment of personalized medicine"

(Cheng C, Ming M et al, 2006). While the radioactive tagging can be considered reliable, it's use has become sparse due to safety considerations on the other hand conventional fluorescence techniques suffer from photobleaching of fluorophores and require cumbersome when analysing when multiplexed signals [3]. Additionally, fluorophores and chemiluminiscent tags generally have broad emission profiles (50-100 nm full width at half-maximum), with chemiluminiscent tags experiencing peak overlap at room temperature [9, 10], which limit the multiplexing capability of these methods.

The development of Surface Enhanced Raman Spectroscopy as a modality for molecular detection has the potential of overcoming many of these challenges and providing a technological platform that can be useful in both remote and real time diagnosis. The initial observation of intense and enhanced Raman Scattering signal of pyridine in 1979 [11] allowed the development of Surface Enhanced Raman Scattering (SERS) technique through which reports of enhancement of upto 10^{14}-10^{15} of the Raman signal have been published [12 - 20]. These kinds of enhancements have been obtained using gold nanoparticles (AuNP) as absorbates for the Raman active molecules [12, 25]. In addition to this single molecule detection has also been observed [21 - 23]. With these developments the initially weak Raman Signal can now be detected and measured even for small quantities of Raman active molecules. One of the most remarkable advantages of SERS lies in the type of spectrum that is obtained by the technique which can be described as multiple sharp "fingerprint" signals (~1 nm fwhm) [24, 25]. Each spectrum contains numerous distinct peaks. The sharp nature of the peaks allows for ease of detection while the number of peaks for the spectrum of each molecule allows for verification hence making it possible to identify the spectrum of one molecule from other molecules in a mixture. The availability of a wide choice of Raman Reporters including

both fluorophores and nonfluorophores allows SERS to overcome the limitation caused by photobleaching. This and the fact that the setup for making Raman measurements can be put together from readily available optical equipment means that SERS has the potential as a quantitative, low cost molecular detection modality.

1.2 <u>Scope of this Thesis</u>

The main objective of this thesis is to provide a molecular imaging platform based on Surface Enhanced Raman Scattering and demonstrate the identification a cancerous cell by detection of a cancer biomarker on the cell.

The specific aims were:

Aim 1: To synthesis and characterize various sizes of spherical gold nanoparticles (AuNP), encode, pegylate and characterize these AuNP to make optimized nanotags usable in multicolor biomolecular detection.

Aim 2: To show that the optimized nanotags can be used in targeting biomolecules *in vitro* by targeting Epidermal Growth Factor receptor in human glioblastoma cells.

1.3 <u>Organization of the Thesis</u>

This thesis comprises of five chapters. The first chapter presents a brief introduction into molecular detection modalities, explaining the choice of Surface Enhanced Raman Spectroscopy as the molecular detection method of choice. It includes the specific aims for the thesis and its general organization.

The second chapter contains three subsections. In the first subsection, Raman Scattering is discussed. A brief explaination, including the classical and quantum basis of the phenomenon is offered. In the second subsection, Surface Enhanced Raman Scattering is discussed along with current observations and explanations given for these observations and in

the third subsection the design of the Raman Modular system used in the research is introduced.

The third chapter discusses the synthesis and characterization of the AuNP and how they are used in the synthesis of Raman nanotags. It includes results for characterization of the of nanoparticle and nanotag and signals obtained.

The fourth chapter describes i*nvitro* targeting of biomolecular receptor. It contains a brief introduction into cancer biomarkers with specific emphasis on EGFr as the biomolecule implicated in the metastasis of brain tumor and a general description of how targeting is done. This is followed by a description of functionalization of the nanotag using anti-EGFr and conjugation of functionalized nanotag onto receptor molecules.

Each of the chapters from chapter three to chapter five is divided into three subsections. On the first subsection a brief introduction is given of the goals of the set of experiments done in the section. The second subsection gives and discusses the results obtained and finally the process is described in the last subsection.

The last chapter gives summarizes and observations and gives a conclusion and recommendations for the system.

CHAPTER 2

SURFACE ENHANCED RAMAN SPECTROSCOPY

2.1 Raman Scattering

When a sample is irradiated by an intense beam of light the scattered light observed usually consists of two types of scattered light. The first one is called Rayleigh Scattering and is normally strong and of the same frequency as the incident light. The second type of scattering is called Raman Scattering. It is named after its discoverer Sir Chandrasekhara Venkata Raman in 1928. It is normally very weak (10^{-5} - 10^{-7})of the incident beam and has a frequency higher or lower than the incident beam). Figure 2.1 below illustrating the two types of scattering for Rayleigh and Raman Scattering for Carbon tetrachloride, CCl_4.
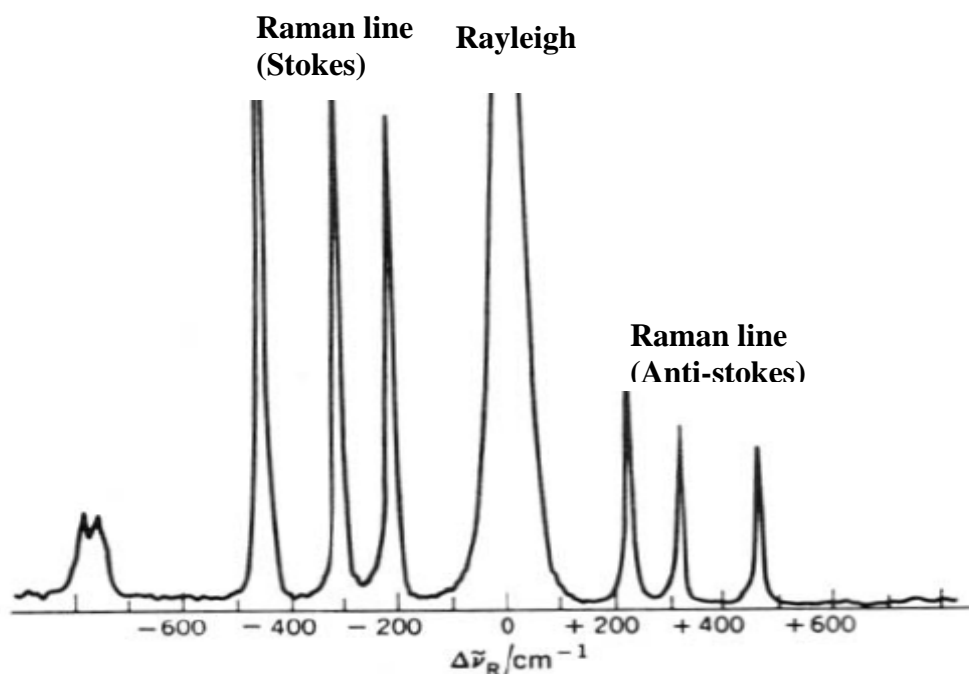
Figure 2.1: Rayleigh Scattering, Stokes and anti-Stokes Raman Spectrum of CCl_4 (488 nm excitation) (Ferraro J R et al, 2003)

Raman Scattering is caused by vibrational, rotational and electronic energy changes in a molecule. These transitions appear in the $10^4 \sim 10^2$ cm^{-1} spectral region. Table 2.1 gives a comparison of various spectroscopic methods and their corresponding spectral regions.

Table 2.1: Spectral Regions and Their origins (Ferraro J R et al 2003)

Spectroscopy	Range($\tilde{v}$,cm^{-1})	Origin
Gamma-ray	10^{10}-10^8	Rearrangement of elementary particles in the nucleus
X-ray	$10^8 - 10^6$	Transitions between energy levels of inter electrons of atoms and molecules
UV-Visible	10^6-10^4	Transitions of energy levels of valence electrons of atoms and molecules
Raman and Infrared	10^4-10^2	Transitions between vibrational levels (change of configuration)
Microwave	10^2-1	Transitions between rotational levels (change of orientation)
Electron Spin resonance (ESR)	1-10^{-2}	Transitions between electron spin levels in magnetic field
Nuclear Magnetic Resonance (NMR)	10^{-2}-10^{-4}	Transitions between nuclear spin levels in magnetic fields.

The classical view of scattering is explained using a dipole. A dipole on a molecular level can be created as a result of electronic excitation or polarizability in the presence of an electric field which can be caused by an incident laser. Considering the simple case of a dipole molecule which has two atoms connected by a single chemical bond as shown in Figure 2.2 below.
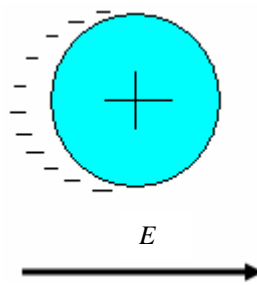
Figure 2.2: A molecule polarized in the presence of electric field E from incident light

.   If a laser light having an electrical field strength, E, incident on a molecule. Since E fluctuates with time and can be written as:

$$E\ (t) = E_o\cos 2\pi v_o t, \qquad\qquad (2\text{-}1)$$

Where E_o is the vibrational amplitude, v_o is the frequency of the laser, the electric dipole moment P of a molecule irradiated by this light is given by:

$$P = \alpha E(t) = \alpha E_o\cos 2\pi v_o t \qquad\qquad (2\text{-}2)$$

Where α is a polarizability.

In the classical sense, a dipole can be viewed as two molecules connected by a single "elastic" chemical bond.
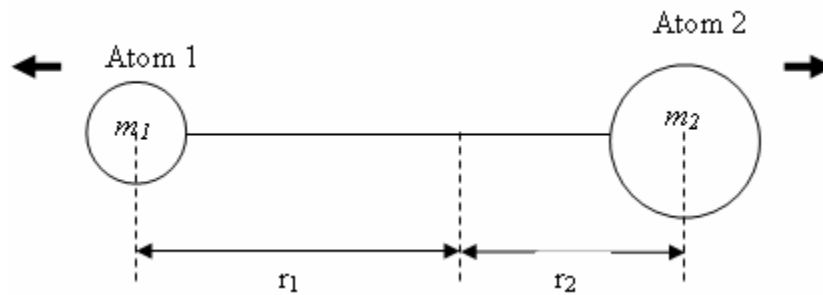
Figure 2.2: The classical concept of a dipole molecule

Vibrational translations in the dipole molecule therefore occur about the centre of gravity. The molecule therefore acts as a harmonic oscillator with a nuclear displacement given by

$$q = q_o \cos 2\pi v_m t \qquad\qquad (2\text{-}3)$$

7

Where q_o is the maximum displacement v_m is the vibrational frequency, t is the time taken. The frequency v_m is given by

$$v_m = \frac{1}{2\pi}\sqrt{\frac{K}{\mu}}$$

(2-4)

Where μ is the reduced mass of the molecule given by

$$\mu = \frac{m_1 m_2}{m_1 + m_2}$$

(2-5)

The quantum-mechanical frequency v_m also take the same form as it classical counterpart except that in this case the energy is quantized and changes only in units of hv.

For small amplitude of vibration, q_o, α is a linear function of q and can be written as:

$$\alpha = \alpha_o + \left(\frac{\partial \alpha}{\partial q}\right)_o q_o + \ldots$$

(2-6)

Combining equations (2-2), (2-3) and (2-6)

$P(t) = \alpha E_o \cos 2\pi v_o t$

$= \alpha_o E_o \cos 2\pi v_o t + \left(\frac{\partial \alpha}{\partial q}\right)_o q\, E_o \cos 2\pi v_o t$

$= \alpha_o E_o \cos 2\pi v_o t + \left(\frac{\partial \alpha}{\partial q}\right)_o q_o\, E_o \cos 2\pi v_o t \cos 2\pi v_m t$

$= \alpha_o E_o \cos 2\pi v_o t + \frac{1}{2}\left(\frac{\partial \alpha}{\partial q}\right)_o q_o\, E_o\, [\cos 2\pi (v_o + v_m)t + \cos 2\pi (v_o - v_m)t]$ (2 - 7)

From the classical theory, the first term represents Rayleigh Scattering. The second term represents Raman Scattering with the term having frequency $(v_o + v_m)$ corresponding to anti-Stokes Raman Scattering and $(v_o - v_m)$ corresponding to Stokes.

For Rotational Raman scattering, the polarizability α is time dependent and can be written as

$$\alpha = \alpha_o + \Delta\alpha \cos 2\pi v_{rot} t$$

(2 - 8)

8
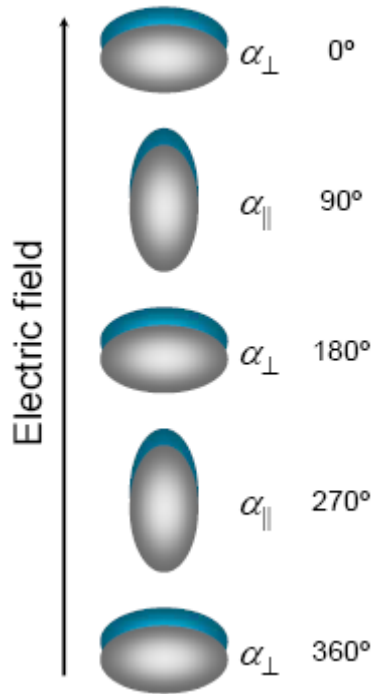
Figure 2.4: Time dependant polarizability of a rotating molecule (Bengtsson P, Bood J, 2008)

Since $\Delta\alpha = \alpha_{ll} - \alpha_{\perp}$ and α ranges from $\alpha = \alpha_o - \Delta\alpha$ to $\alpha = \alpha_o + \Delta\alpha$ with the rotating molecule

$$P(t) = \alpha\vec{E}\cos 2\pi v_o t$$
$$= (\alpha_o + \Delta\alpha\cos 2\pi v_{rot} t)\vec{E}_o \cos 2\pi v_o t \qquad (2\text{ - }9)$$
$$= \alpha_o\vec{E}_o \cos 2\pi v_o t + \frac{1}{2}\vec{E}_o\Delta\alpha\{\cos 2\pi(v_o + 2v_{rot})t + \cos 2\pi(v_o - 2v_{rot})t$$

In this equation 2-9 again the first term represents Rayleigh scattering, the second term represents anti-Stokes Raman scattering and the third represents Stokes Raman scattering.

From an electronic stand point, scattering can be visualized as the transition of an excited electron(s) to a virtual state. When the electron comes back to ground state it emits radiation which has equal frequency as the incident light. This is the cause of Rayleigh scattering. However, in some cases the electron will return to level higher than the original level

9

in ground state resulting in Stokes Raman scattering, or a level lower than the original level at ground state (anti-Stokes Raman Scattering).
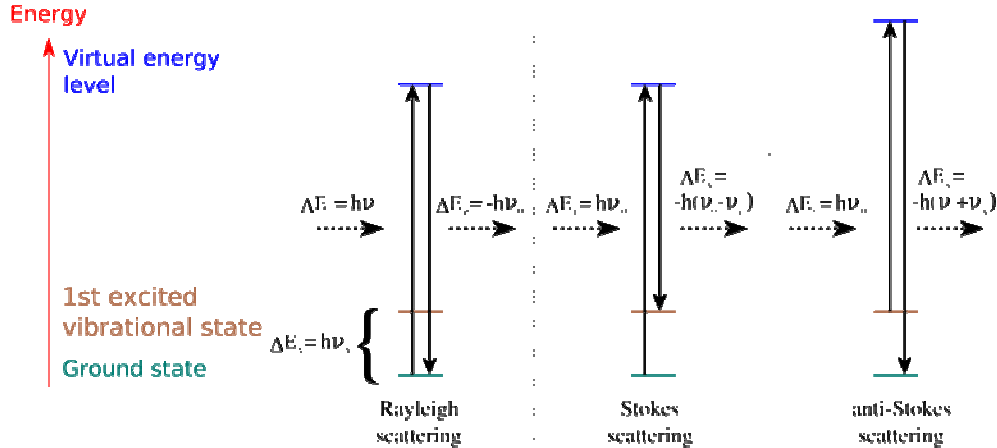
Figure 2.5: Energy level diagram of Stokes and Anti-Stokes Raman Scattering (Annabel, English Wikipedia [http:/ / en.wikipedia.org/ wiki/ Image:Ramanscattering.png])

2.2 Surface Enhanced Raman Scattering

From the equation (2 - 5) it is clear that any enhancement of the Raman Signal must come from an enhancement in α (molecular polarizability) and/or from electric field E since intensity of Raman scattering is proportional to the square of the Electric dipole moment P [26]. Surface Enhance Raman Scattering can therefore be said to be due to two separate effects. A long range electromagnetic effect, which involves the enhancement of the electric field, and a short range chemical effect, that occurs for only those molecules that are chemisorbed on the surface [29].

Electromagnetic effect depends on a localized surface plasmon and therefore requires electron rich metals like gold and silver. When light it incident on a metal surface, the localized plasmon field is excited. The greatest enhancement occurs when the field of enhancement is in resonance with the incident radiation i.e. when the frequency of irradiation light approaches the frequency of oscillation of the surface plasmon. Surface Enhance Raman Scattering can be

10

explained as a double enhancement explaining why such large values of enhancement are observed.   First the incident electromagnetic radiation is enhanced by the plasmon field as it irradiates the molecule.   The scattering from the molecule then gets enhanced by the same mechanism resulting in an E^4 enhancement of electric field.   It is also important that the plasmon field oscillates perpendicular to the surface. Therefore rough surfaces, which increase the probability of such orientation, are preferred.

Short range enhancement on the other hand is enhancement caused by a change in the molecular polarizability. It normally occurs for only those molecules that are chemisorbed onto the surface of an electron rich molecule and is due to quantum size confinement. When particle gets smaller and smaller it's energy levels get more and more quantized. The energy required or released during transitions increase. For very small molecules, the energy levels can be called HOMO and LUMO.   When such a molecule is chemisorbed onto an electron rich metal surface so that its HOMO and LUMO fall in the Fermi-level of the adsorbate,   the adsorbate acts as an electron transfer intermediate allowing for easier transitions between the HOMO and LUMO transitions and therefore enhancing the signal.

2.3 Surface Enhanced Raman Spectroscope Setup

Figure 2.6 illustrates a schematic representation of the setup used in the experiments for detection of the Surface Enhanced Raman Spectrum. The setup consists of four main parts: the excitation source, a modular sample illumination and collection system, the spectrometer and detector unit and processing computer system.

The excitation was a 785 nm laser SIFC780 laser (Thorlabs) fiber coupled to the illumination system. The advantage of using 785 nm laser is the fact that it falls within the optical window. This would allow for less noise in the signal due to autofluorescence and also reduce absorption of light by water.

11
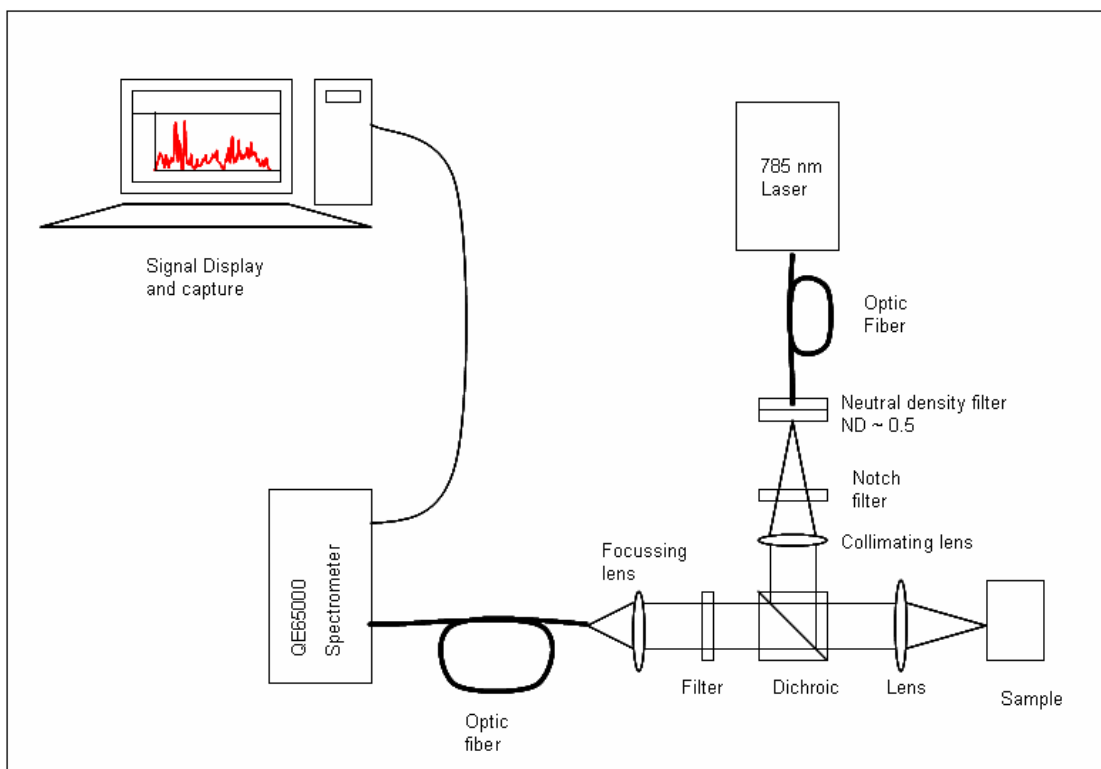
Figure 2.6: Schematic of the Surface Enhanced Raman (SERS) Setup

The illumination and collection module is made up of two arms connected perpendicular to each other.   Light from the laser is coupled onto the illumination arm using a multimode optic fiber. The power of the laser is controlled using an neutral density filter (~ 0.5) at the entrance of the illumination arm, then its band width is narrowed using a notch filter. A dichroic located at the intersection point of the two arms reflects the incoming light to a focusing lens onto the sample platform. In this setup the focusing lens used is 40x lens (Carl Zeiss) since the setup was mounted onto a microscope for simultaneous visualization of cells as Raman spectrum is recorded.

Raman scattering is collected in a reflection geometry which is convenient if the if the system is to be modified for *invivo* applications. The reflected light is transmitted through the dichroic and filtered before being focused by a lens onto a multimode optical fiber connected to a QE65000 spectrometer (Ocean optics) which uses a Hamamatsu s7031-1006 detector.

Versatility of the modular system allows it to be able to be detached transported and work compatibly with a variety of instruments or as a stand alone setup.
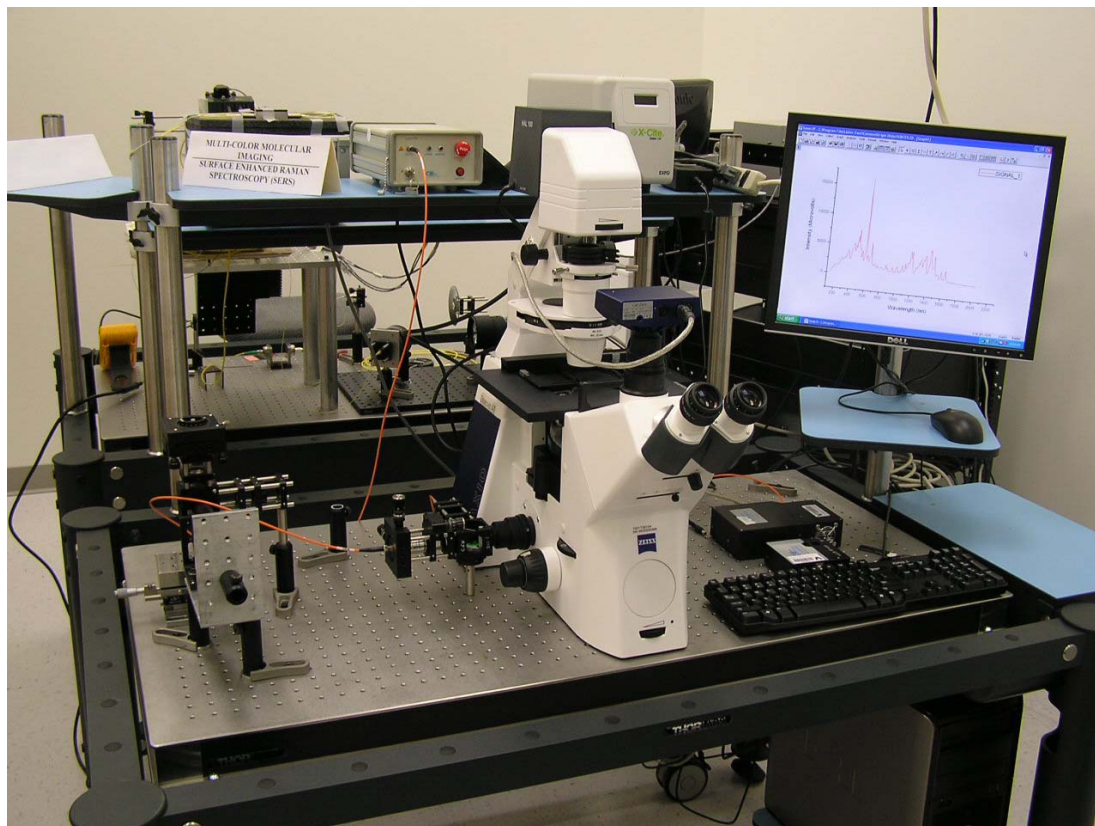
Figure 2.7: Raman Module Connected to Microscope

Figure 2.7 is a picture of the current setup where the modular system is connected to a microscope for simultaneous observation of cells and detection of Surface Enhanced Raman spectrum.

CHAPTER 3

SYNTHESIS AND CHARACTERISATION OF RAMAN NANOTAGS

3.1 <u>Raman Nanotags</u>

In the recent years, designs of Raman nanotags have included the use of metal nanoparticles or nanotubes [30]. Many of these designs involve encoding the nanoparticles or nanotubes and then encapsulating them in a coating of polymer or glass [30 - 32]. Three main advantages have emerged as a result of this coating. To begin with the coating protects the nanoparticles from the effects of "harsh" solvents making them stable, secondly the coating secures the dye onto the surface of the gold, hence protecting the target cells from any effect that might result from exposure to the dye and finally it has been observed that nanoparticles or nanotubes that are coated in this way remain longer in circulation than plain nanoparticles in small living animals [32, 33].

The most common metals used in the making of nanotags are copper, silver and Gold [30 - 33]. Copper is commonly used in the synthesis of nanotubes, whereas silver and gold are common in nanoparticle synthesis. For biological environments the reported biocompartibility of gold make it preferred for the synthesis of nanotags. Gold has been used for centuries in dentistry, as an antipruritic and for over 50 years in the treatment of Rheumatoid Arthritis [34, 35]. While some rare side effects have been reported, studies have indicated that these are due to trivalent gold formed as a result of oxidation of the gold salts used, whereas metallic gold shows no evidence of clinical or laboratory toxicity [36 - 38]. In addition not only are AuNP known to optically enhance the Raman signal, this enhancement is size dependent. Reports indicate that optimal SERS in the Near Infrared (NIR) would require silver nanoparticles with diameters greater than 200 nm, while SERs for AuNP are optimized at 60 – 65 nm [22, 31, 37]. This means that smaller sized nanoparticles are available for use increasing the specificity of

14

targeting biomolecules. Finally, the chemical synthesis of gold nanoparticles is also relatively simple and reproducible increasing the convenience in the synthesis of the nanotags.

The positively charged and or thiolated Raman reporter dyes readily attached to the AuNP through physioadsoption and chemiadsoption respectively. Using this property it is possible to select a wide range of fluorescent or nonfluorescent Raman reporters.

This section describes the synthesis AuNP using Fren's Method and the seed growing method and their characterization. The nanoparticles are then used to synthesis Raman nanotags . It is confirmed that the optimal AuNP size for SERS at 785 nm laser irradiation is 60 – 65 nm. In addition, the coating on the AuNP has a effect on the Raman signal since the citrate coated nanoparticles give higher yield than the nanoparticles coated with 2-mercaptosussinic acid (MSA). The encoded nanoparticles, when further encapsulated in thiol modified polyethylene glycol (mPEG-SH) and thiol modified heterofunctional polyethylene glycol (HS-PEG-COOH) collectively called PEG coating, remains stable even under "harsh" conditions and the SERS signal remains strong for months. In addition the signal before and after peglyation remained similar within the range of uncertainty indicating that mPEG-SH did not displace the Raman reporter dye. This was consistent with observations reported by Qian X et al, 2008. The value of HS-PEG-COOH is that it provides sites for functionalization of the nanotag with biomolecular targeting ligands, such as antibodies, and peptides target cancerous cells or other cells of interest with high specificity and affinity [39 - 41]. Finally, five different color nanotags are described. The distinctness and number of their peaks allows for potential use in multiplexing.

3.2 Synthesis and Characterization of gold nanoparticles and nanotags

3.2.1 Synthesis of Gold nanoparticles

Six sizes of gold nanoparticles were synthesized using two methods: the Frens method [42 - 44] and the seed growth method by Jiali Niu [45].

Table 3.1 shows the details for the AuNP synthesized using the Frens method. Two different sizes were synthesized, one of 16.7 ± 1.2 nm and the second of 65.6 ± 6.4 nm. The

15

sizes were determined by calculation and confirmed using Transmission Electron Microscope and Dynamic Light Scattering as shown in figure 3.1 and 3.2 respectively.

Table 3.1: Details for AuNP synthesized using Fren's Method

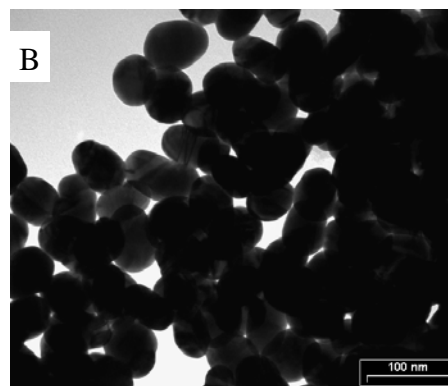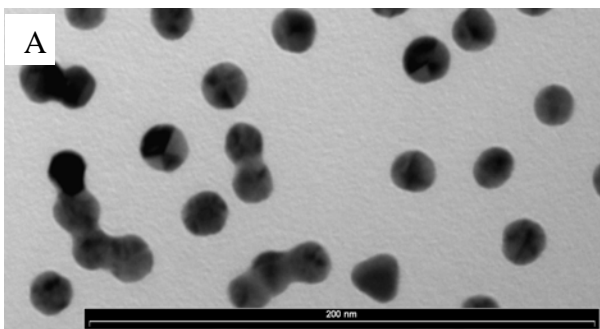| Set No.	HAuCl$_4$ Volume/conc.	1% (wt) Citrate Volume (µl)	Diameter (nm)	AuNPs con. (nM)	AuNPs /l
Citrate1	50 ml	1750	16.7±1.2	1.61	9.70 x 10^{14}
Citrate2	2.5 × 10^{-4} M	400	65.6±6.4	1.10	6.60 x 10^{14}

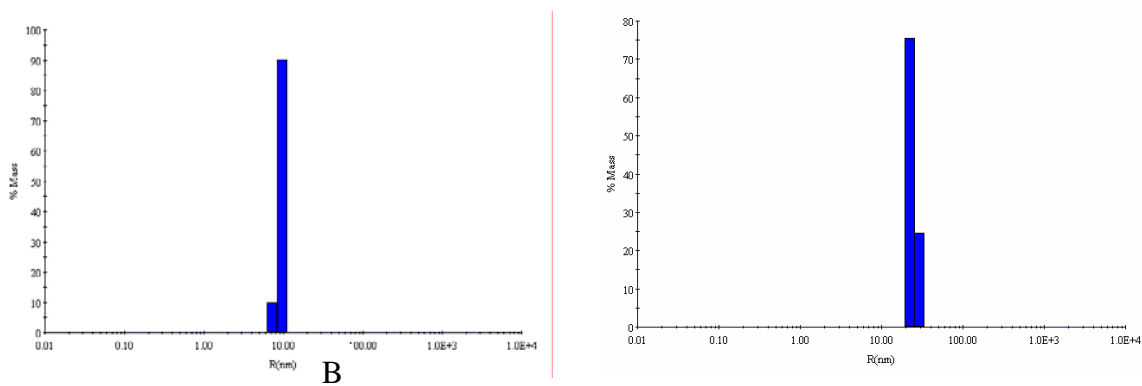Figure 3.1: TEM images of (A) citrate-1 and (B) citrate-2 nanoparticles

Figure 3.2: DLS measurements of (A) citrate-1 and (B) citrate-2 nanoparticles

Comparison of the TEM images and DLS results of the synthesized nanotags showed consistent size correlation for the citrate-1 gold nanotags, however, for citrate-3 the DLS measurement of radius was significantly lower than measurements obtained from the TEM images. This is probably due to the fact that the citrate-2 nanoparticles are not perfectly spherical and such effects are magnified in bigger particles.

Using citrate-1 nanoparticle as seeds and MSA as a reducing agent, nanoparticles in the size range ~ 50 – 120 nm were synthesized according to the one step seeding growth approach described by Jiali Niu [45]. In this method different amounts of gold seeds are added while with keeping the amount of chloroauric acid (HAuCl$_4$) constant. In this way a thinner gold layer forms when seeds are many, but the gold layer is thicker when the gold seeds are fewer. Table 3.2 below shows the details for the different AuNP synthesized.

Table 3.2: Details for AuNP synthesized by seeding growth method

Set No.	$V_{Au-seed}$ (µl)	M_{seed} (µM)	M_{HAuCl4} (µM)	Diameter (cal.) (nm)	Diameter (nm)	Concentration (AuNPs/l)*
Seed	—	250		—	16.7±1.1	—
MSA-1	400	2		59	51±3.1	3.01 x 10^{13}
MSA-2	200	1	80	68	65±3.6	8.94 x 10^{13}
MSA-3	100	0.5		92	83±5.1	1.67 x 10^{14}
MSA-4	40	0.2		125	114±7.9	3.66 x 10^{14}

Measurements from the TEM images and the DLS results for citrate-1 nanoparticles held close agreement with each other. In addition comparison between the shapes of these nanoparticles to citrate-2 nanoparticle revealed more regular shaped nanoparticles for citrate-1. This suggests that the one step seed growing method is better for size and spherical shape control during synthesis of nanoparticle.
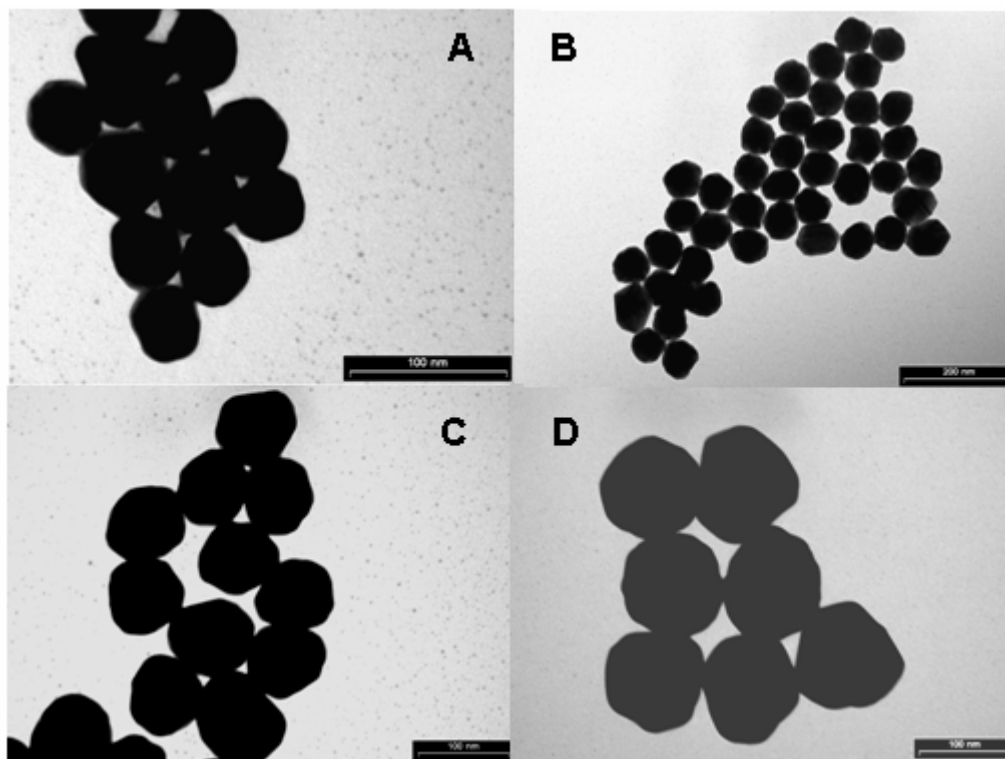
Figure 3.3: TEM images of gold nanoparticles made using Jian Niu's method and coated with MSA. The nanonoparticles are of (A) 51±3.1 nm, (B) 65±3.6 nm, (C) 83±5.1 nm and (D) 114±7.9 nm
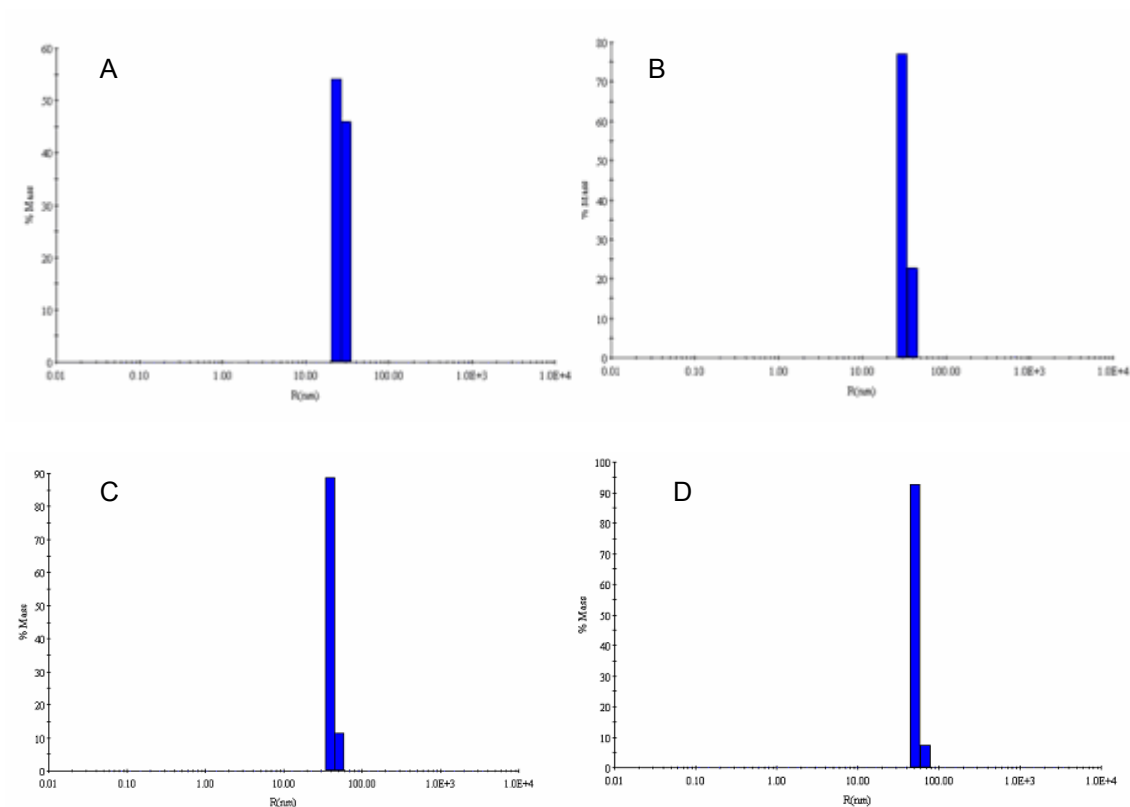
Figure 3.4: DLS measurements of gold nanoparticles made using Jian Niu's method and coated with MSA. The nanonoparticles are (A) 51±3.1 nm, (B) 65±3.6 nm, (C) 83±5.1 nm and (D) 114±7.9 nm

3.2.2 Synthesis of Nanotags

Synthesis of the nanotags involved encoding the nanoparticles with the Raman reporter and coating the encoded nanoparticles with a protective layer of mPEG-SH and HS-PEG-COOH. Figure 3.5 illustrates the schematic for the process of synthesis of Raman nanotags and figure 3.6 shows an example of SERS signal obtained from the synthesized nanotag. Nanotags are optimized to give the highest signal while minimizing aggregation of gold nanoparticles and having sites that for functionalization.
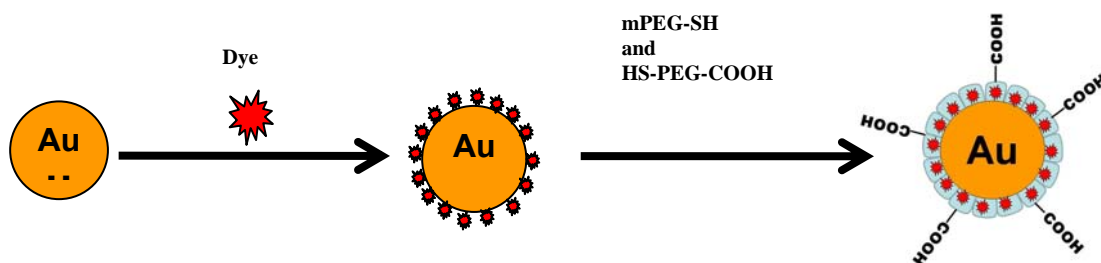
Figure 3.5: Schematic drawing of the process of nanotag synthesis

The kind of signal obtained from the nanotag clearly indicates an enhanced signal. This is confirmed by the observation that the signal obtained in a plain solution of the Raman reporter did not yield a distinguishable signal above the background. The presence of a strong signal is also indication that the Raman reporter is adsorbed onto the gold nanoparticles, since for SERS to take place, the molecule of interest has to be within a limited sensing distance of the metal surface.
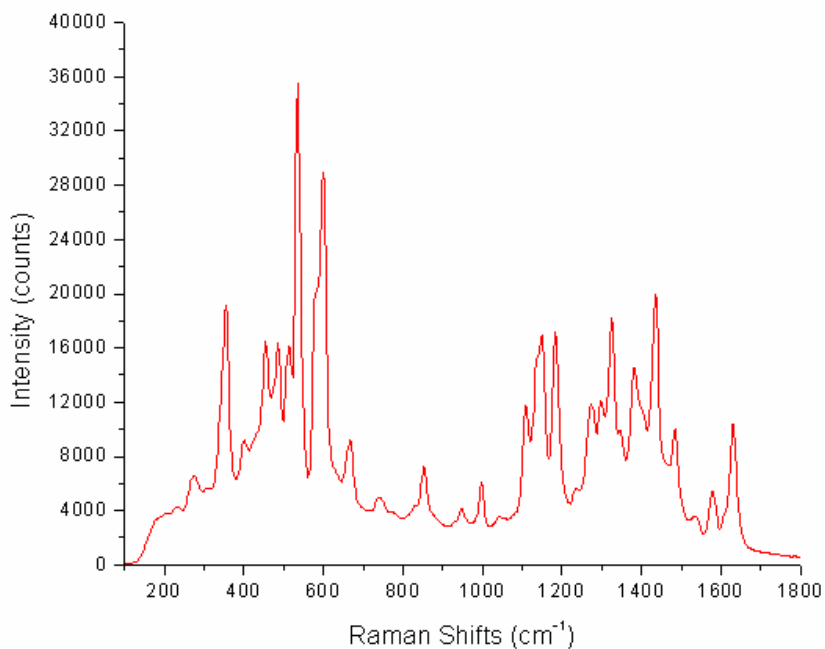
Figure 3.6: Surface Enhanced Raman spectrum of Cresyl Violet

20
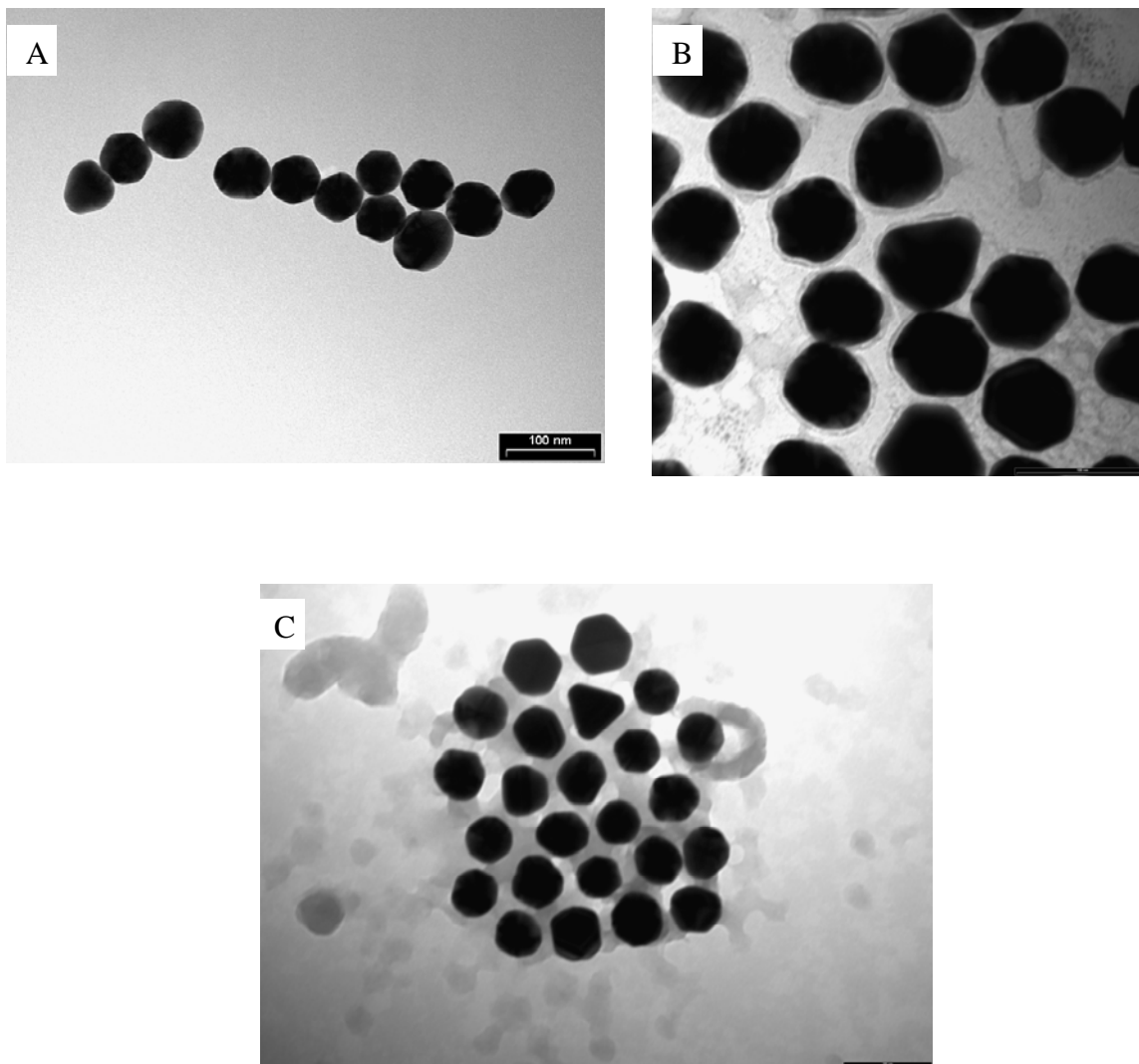
Figure 3.7: TEM pictures of (A) plain gold nanoparticles, (B) monodispersed nanoparticles coated with PEG and (C) nanoparticles in a matrix formed by PEG coating

Figure 3.7 (B) illustrates the end product of nanotag synthesis. A 5 nm PEG coating can be observed from the TEM images of the nanotags. These nanotags are clearly distinguishable from AuNP in figure 3.7 (A). An additional phenomenon is observed in some cases where the PEG coating seemed to form a matrix with nanoparticles incorporated inside. In order to minimize this effect and obtain as many single nanoparticles coated with

polyethylene glycol as possible, addition of the polyethylene glycol is done while the gold solution is rapidly mixing.

UV-Vis spectroscopy provided further confirmation through the obwervation of a 3 nm shift in the plasmon peak that was always observed after the encoding and pegylation process.
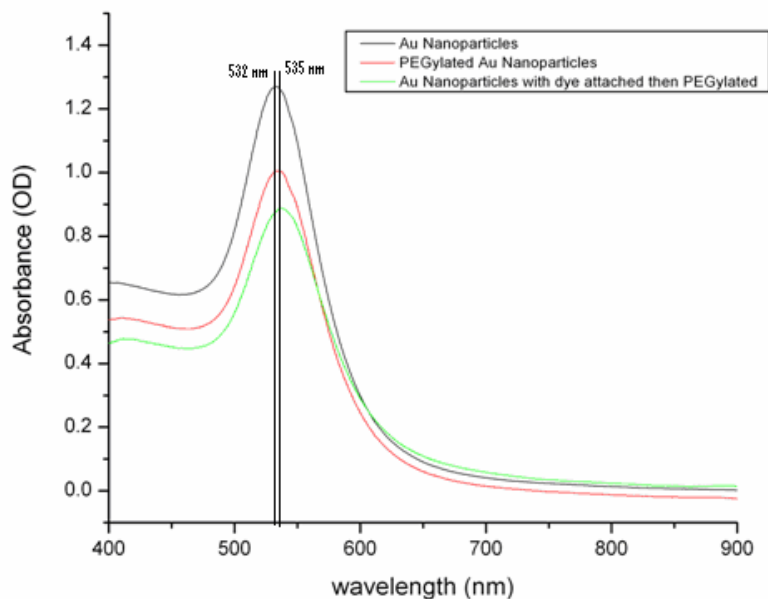
Figure 3.8: Comparison between UV-Vis spectra of AuNP and Nanotags showing a 3 nm plasmon shift

A final confirmation of PEG coating is observed when the nanotags are tested for stability by centrifugation and resuspention in different solvents including Potassium Phosphate Buffer, MES, Goat serum, methanol and DMSO. The nanotags proved stable in all the environments mentioned. Specifically the result that the nanotags remained stable in serum is of importance as it indicates usability of the nanotags in biological environments. Figure 3.9 illustates the effect of PBS on AuNP and nanotags. The AuNP aggregate upon centrifugation and resuspension in PBS, as can be seen on the TEM image figure 3.9 (B), however, the nanotags remain stable even after resuspension in PBS.

Figure 3.9: (A) UV-Vis spectra of AuNPs and nanotags showing the effect of PBS on them and (B) aggregated AuNP upon addition of PBS
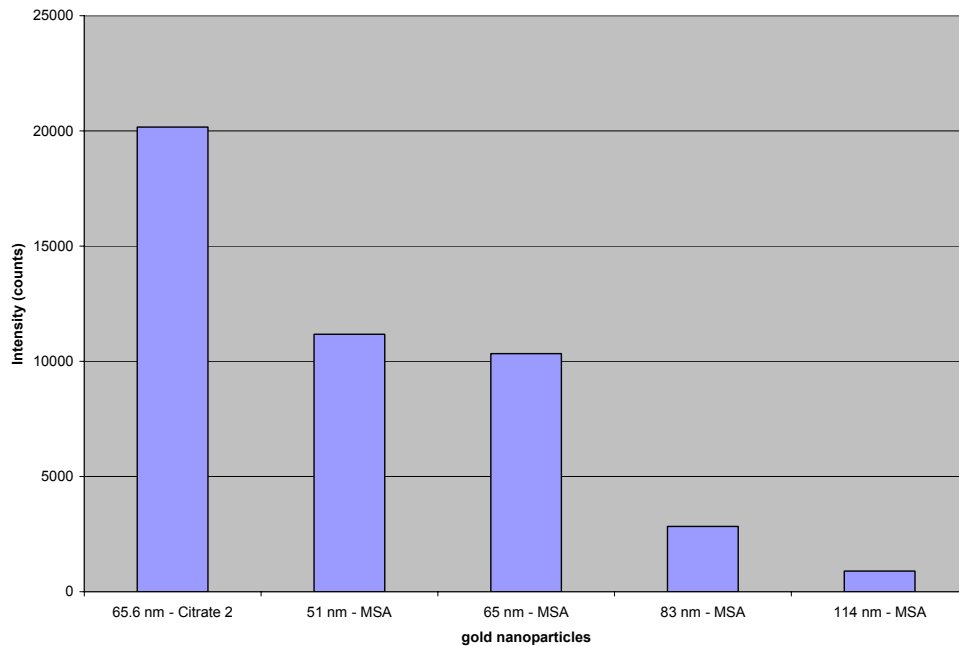
Figure 3.10: Comparison of thhe intensity of the 587.73 nm peak of Cresyl violet for various sizes and types of AuNPs

SERS of five of the six sizes of nanotags were compared to find out the best size for use with the 785 nm laser for Raman measurements by comparing the 583.73 nm Cresyl violet peak intensity of the different spectra for different batches of nanoparticles as shown in figure 3.10. it was found that the best size range amon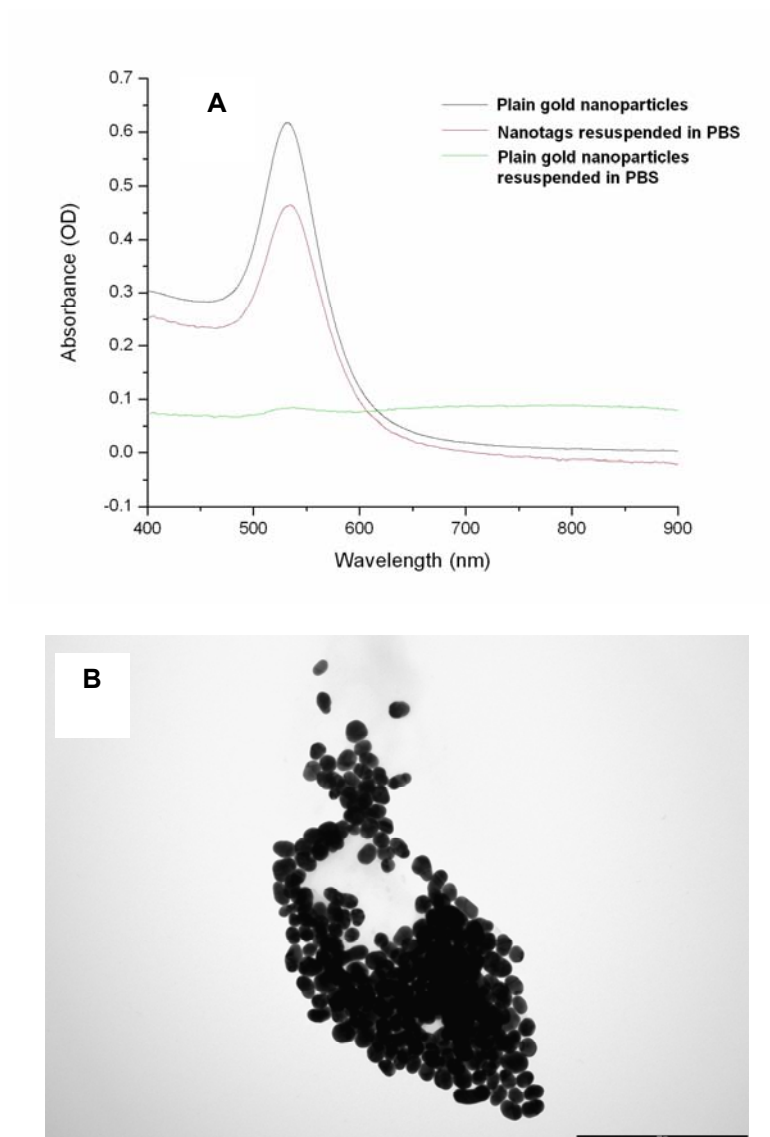g the particles coated with MSA was 51 nm and 65 nm particles. Comparing the citrate-2 and MSA nanotags, results indicated that a stronger signal is obtained using the citrate-2 nanotags. This was probably due to the citrate coating that might be more easily displaced by the dye molecules than the MSA coating. This displacement would allow more dye molecules to be adsorbed onto the gold surface. In addition, the citrate-2 nanoparticles were generally less spherical than the MSA coated nanoparticles. This would allow for greater aspect ratio resulting in greater value of molecular polarizability and therefore causing greater enhancement of the Raman Signal.

Finally, using this method, five different nanotag solutions were made each distinguished from the other by the Raman reporter used in the synthesis. The nanotags used

24

were Cresyl violet, Crystal violet, Rhodamine 6G, DTTC iodide and Nile blue. These dyes were chosen because they have net positively charged molecules. This property is important for adsorption of the dye molecules on the net negatively charged AuNP. In addition, to this property, the presence of thiol group or sulfur on the dye molecules improves adsorption of the molecules. However, it was noted that the PEG coating does not displace the adsorbed Raman reporter molecules since the SERS signal does neither significantly reduce in strength before and after PEG coating.

Table 3.3: Dyes and their Raman Spectra
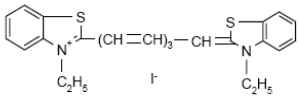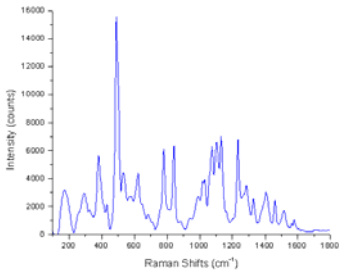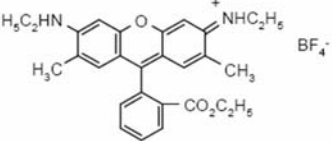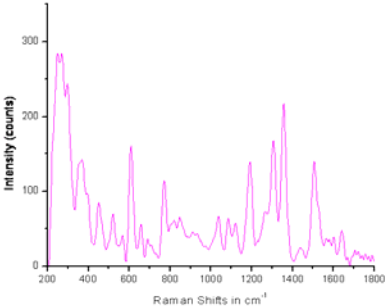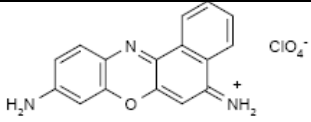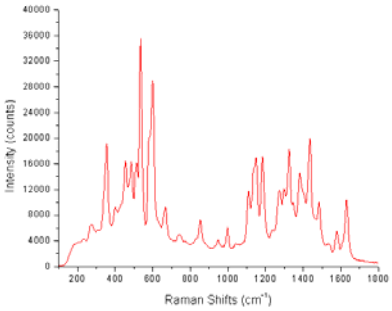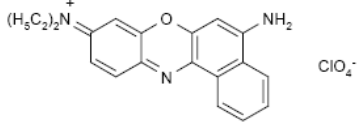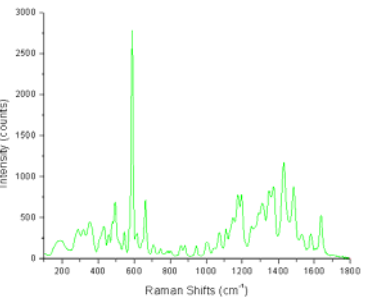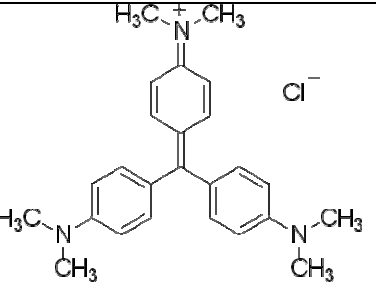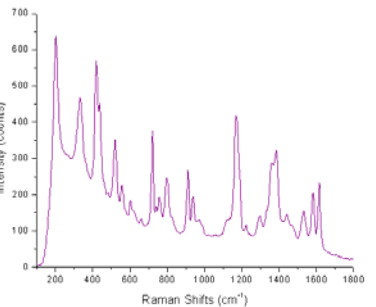
Raman Reporter	Structure Raman Reporter	Raman Spectrum
DTTC Iodide	3-ethyl-2-[7-(3-ethyl-2(3H)-benzothiazolylidene)-1,3,5-heptatrienyl]-benzothiazolium iodide	
Rhodamine 6G Tetrafluoroborate	2-[6-(ethylamino)-3-(ethylimino)-2,7-dimethyl-3H-xanthen-9-yl]-benzoic acid, ethyl ester, Tetrafluoroborate	

25

Table 3.3 - *continued*

Cresyl Violet 670	5-imino-5H-benzo[a]phenoxazin- 9-amine monoperchlorate	
Nile Blue 690 percholate	5-amino-9-(diethylamino)- benzo[a]phenoxazin-7-ium perchlorate	
Crystal Violet		

The power of having multicolor nanotags come from the ability to distinguish two or more nanotags in a mixture. When two nanotag solutions encoded with different Raman Reporters were mixed and the mixture compared against the spectra of both Raman reporters overlapped over each other, each of the Raman reporters are clearly identifiable using multiple peaks. Figure 3.12 shows the possibility of distinquishing two dyes from a mixture.
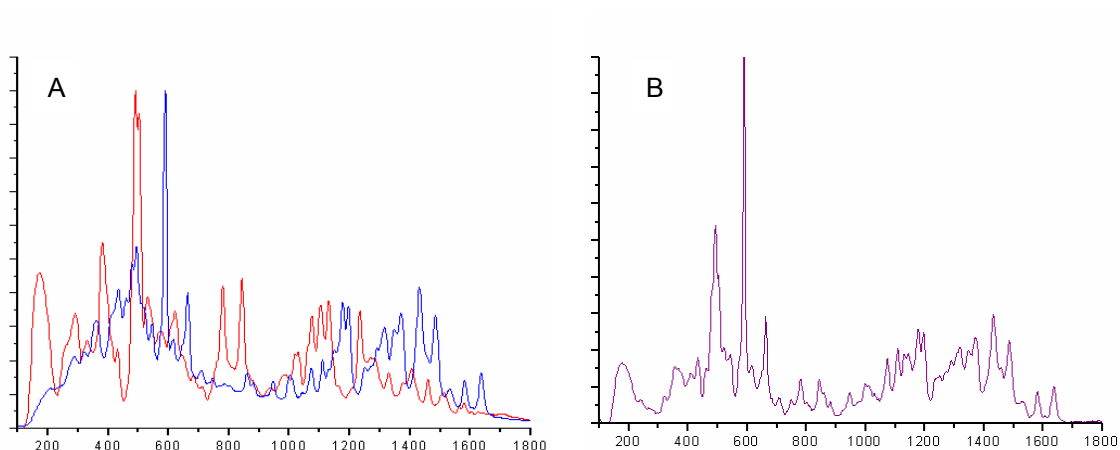
Figure 3.11: Comparison between (A) overlapped Raman Spectra of two Raman reporters and (B) the spectrum of the mixture of the two reporter

3.3 Materials and Methods for Synthesis of Nanotags

3.3.1. Materials

All chemicals, solvents, and reagents were purchased from Sigma-Aldrich and used as received unless otherwise noted. HS-mPEG and HS-PEG-COOH were purchased from Laysan Bio Inc. (Arab, AL). 2-mercaptosuccinic acid (MSA) was purchased in its acid form, whereas it was used in its disodium salt form by NaOH neutralization, therefore the term 'MSA solution' refers to this neutralized solution. Milli-Q water (18 MΩ-cm) was obtained from a Millipore Gradient Milli-Q water system (Billerica, MA). 1-ethyl-3-[3-dimethylaminopropyl]carbodiimide hydrochloride (EDC) and N-hydroxyfulfosuccinimide (sulfo-NHS) were purchased from Pierce Biotechnology.

The hydrodynamic size and size distribution of the AuNPs were measured by a Wyatt's DynaPro dynamic light scattering (DLS) system (Santa Barbara, CA).

The morphology and size of AuNPs were examined by the FEI Tecnai G2 Spirit BioTWIN Microscope (TEM) system (Hillsboro, OR). TEM samples were prepared by placing a drop of fresh gold colloids bearing different size on Cu grids, followed by solvent evaporation at room temperature.

Raman spectroscopy is done using a 785 nm SIFC780 laser (Thorlabs) fiber coupled onto an in-house built Raman module. The spectrometers used for Raman measured and absorbance measurements are Ocean optics QE65000 and USB4000.

3.3.2 Synthesis of Nanoparticles using Fren's Method

An aqueous solution containing 50 ml of 2.5×10^{-4} M $HAuCl_4$ was heated to boiling with stirring; then 1.75 ml 1% (wt) aqueous sodium citrate was added all at once. Within 15 s of boiling, the solution turned faint blue. Under continuous stirring condition, after 45 s, the blue color suddenly changed to red, indicating the formation of AuNPs. The boiling and stirring were continued for 30 min. The seed solution was cooled to room temperature. This method produced AuNPs with a mean diameter of 16.7±1.1 nm according to TEM images. These nanoparticles were named "citrate-1". The concentration of gold seeds was estimated to be 1.1×10^{15} particles/l, assuming all the added $HAuCl_4$ was consumed. By reducing the volume of 1% (wt/v) sodium citrate to 400µl, larger nanoparticles of 65.6±6.4 nm with the concentration 2.87×10^{13} nanoparticles/l called "citrate-2" were synthesised. Concentration of nanoparticles were tuned by centrifugation.

3.3.3. Growth of gold seeds

To get AuNPs with different sizes, 50 ml of the growth solution was added, to each of four 125 ml conical flasks, which contained 240 µl of 0.01 M MSA solution and 160 µl 2.5×10^{-2} M $HAuCl_4$, so that the [$HAuCl_4$]:[MSA] ratios remained constant which was 5:3. Then, different volumes of gold seed solution (400, 200, 100 and 40 µl) were added under rigorous stirring, making the [$HAuCl_4$]: [seeds] ratios 40:1, 80:1, 160:1, and 400:1, respectively. The colour of the reaction mixtures turned from pink to purple in several minutes, indicating the growth of gold seeds. With the above recipes, the calculated mean diameters of the resultant particles were 59, 68, 92, and 125 nm, respectively. Gold colloids prepared by this approach were stable for months. Sedimentation was occasionally found, especially in samples with larger particles, while the precipitate could be easily redispersed with a gentle shake; and the mean diameters of AuNPs could be well maintained.

28

During this reaction different doses of gold seeds were added. The more seeds added, the thinner gold layer would grow onto the surface of gold seeds because the same dose of HAuCl$_4$ was added. Through this methods we could get AuNPs with very uniform size in the range ~50-120nm. AuNPs were protected by MSA through Au-S. It was reported that these particles could be kept in refrigerator for one year without aggregation [19].

3.3.4. Synthesis of Raman nanotags

To prepare the Raman nanotags, freshly prepared Raman Reporter was added to the nanoparticles (2.6 x 10^{13} particles /l). The molarity of the varied from Raman reporter to Raman reporter ranging from 5 uM to 15 uM and was optimized to obtain solution that are as equal in volume as possible. The dye is added in a ratio of about 1:6, however, this is done under constant testing in order to obtain as SERS signals that are consistent from batch to batch. The rate of addition and speed of mixing were also found to be of importance in optimization of the nanotag signal at minimal aggeragation. Stabilization of the nanoparticles is done first adding HS-PEG-COOH (1uM) dropwise to the encoded rapidly mixing encoded gold nanoparticles in the ratio 2:7 by volume, then HS-mPEG (10 uM) is added in a ratio of about 1:6 of the volume of the nanoparticles excess.

29

CHAPTER 4

CELL STUDIES

4.1 <u>Cancer Biomarker: Epidermal Growth Factor receptor (EGFr)</u>

Epidermal growth factor receptor (EGFr) is a 170 kDa transmembrene glycoprotein that acts as a cell surface receptor for various ligands including those of the epidermal growth factor family and Transforming growth factor alpha (TGFα). Under normal conditions, the binding of EGFR to these conjugate ligands results in autophosphorylation of the receptor's intrinsic tyrosine kinase which in located in the intracellular domain of the molecule. Phosphorylation of the tyrosine kinase leads to activation of signal transduction pathways involved in regulation of cellular proliferation. However, overexpression of EGFR results in upregulation of these pathways resulting in increased DNA synthesis, cell proliferation and differentiation [46, 47]. Studies have shown that the overexpression of EGFR is an important marker of poor prognosis of brain tumors. For example 90% of high-grade astrocytic gliomas express EGFR which is associated with EGFR gene amplification in 40 – 50% of glioblastoma multiforme (Kuan et al 2001) [48].

The monoclonal anti-human EGFR, clone H11 (anti-EGFR) is a ligand that displays high specificity to wild type EGFR (MW 170 kDa) and can be used in Western blot as well as in immunofluorescence as the primary antibody.

In this section, anti-EGFR, is used to target EGFR receptors in tumor glioblatoma cells and normal ones. The aim is to determine the qualitatively if the SERS system can detect the difference in expression level between the two types of cells and therefore build a basis for quantification of expression levels of EGFr. The method used is the generally method for staining in immunocytochemistry, except that the primary anti-EGFr is replaced with nanotags functionalized with anti-EGFr and a secondary antibody anti-IgG with a fluorescent tag is added

30

to confirm binding of the nanotags. The results indicate that conjugation seems to occur and SERS signals are obtained. It is possible to see the signals between the tumor and the normal cells. However, there is high Signal to Noise ratio (SNR).

4.2 *Invitro* targeting of Cancer Biomarker

Figure 4.1 illustrates the 8 well "plate" made from glass cover slip and polydimethylsiloxane (PDMS) stamp that is used in the testing of cells
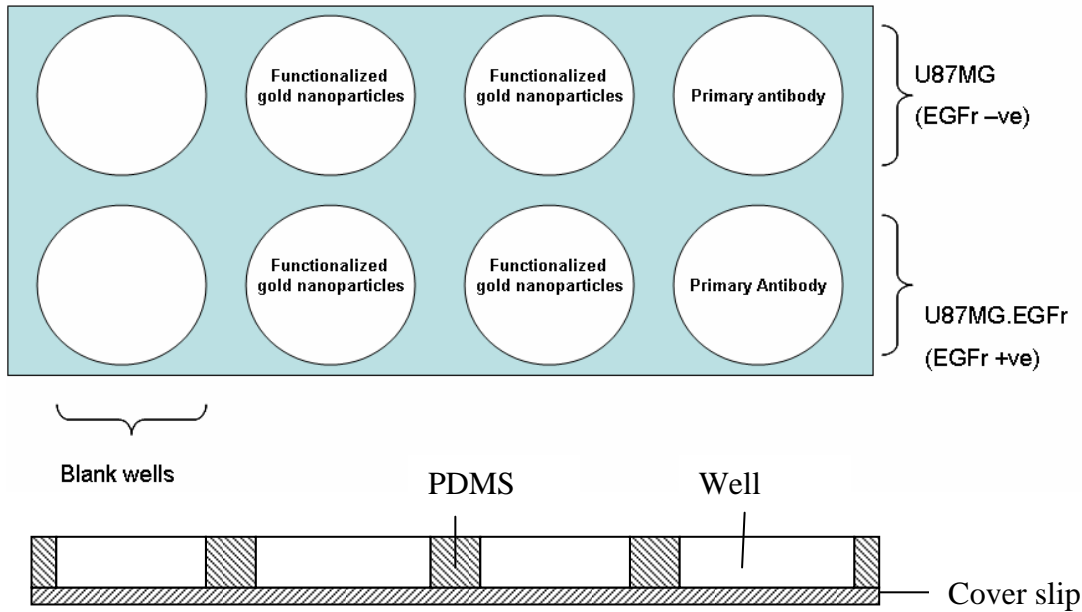
Figure 4.1: The stamp used for the cell studies. (A) is the ariel view and (B) shows the cross-sectional view. The labeling inside the wells indicate the "primary" either antibody or nanotag introduced

The procedure involved functionalization of nanotags, blocking the cells, nanotag conjugation and staining using secondary attached to a fluorescent dye. In this case, since the primary was mouse anti-Human EGFr (U87), the secondary used was goat anti-mouse IgG Alexa Fluor 594. In figure 4.1 (A) the wells are labeled with the primary that was introduced to the cells.

31

A

B

C

D
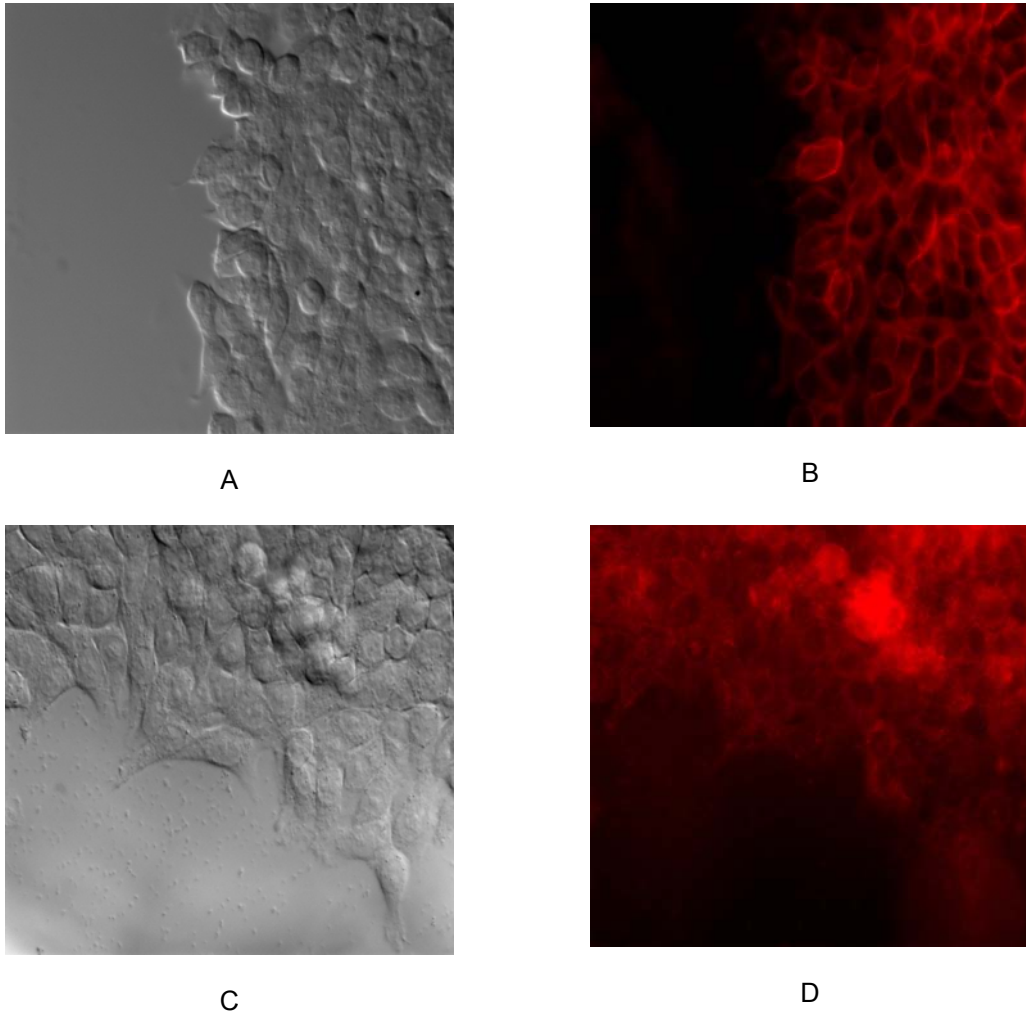
Figure 4.2: (A) DIC images and (B) Fluorescence images of cells that overexpress EGFr and have been tagged with functionalized gold nanotags and then labeled using goat anti-mouse IgG –Alexa 594 (C) and (D) are similarly treated but for the cells that express EGFr at normal levels

In both figures 4.2 (B) and (D), the fluorescence is observed showing presence of secondary in the cells which indicate that nanotags attach to the cell expressions on the cell walls of cells in those wells. Figure 4.3 and figure 4.4 also confirm this by showing that the secondary antibody anti-IgG is very specific to the antibody and does not attach significantly in the absence of the primary antibody.
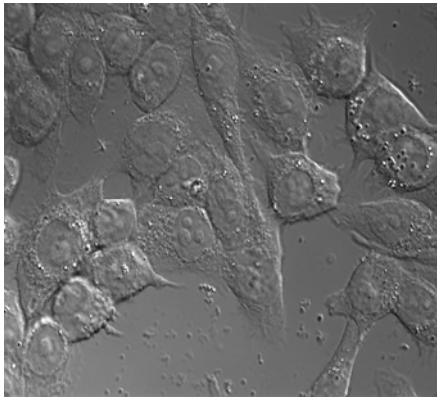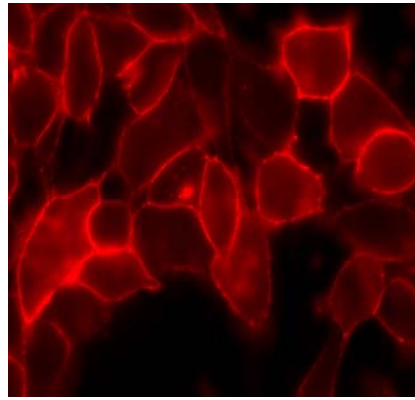
A
B

Figure 4.3: (A) DIC images and (B) Fluorescence images of cells that overexpress EGFr and have been tagged with mouse anti-Human EGFr and then labeled using goat anti-mouse IgG – Alexa 594

Comparison of SERS in the cancerous cells and normal shows a difference in SERS signals. However, the signal to noise level between then is low. This could be caused by a poor efficiency in binding of the nanotags due to low yield in functionalization hence reducing the population of cells available for conjugation with the EGF receptors on the cell surface.
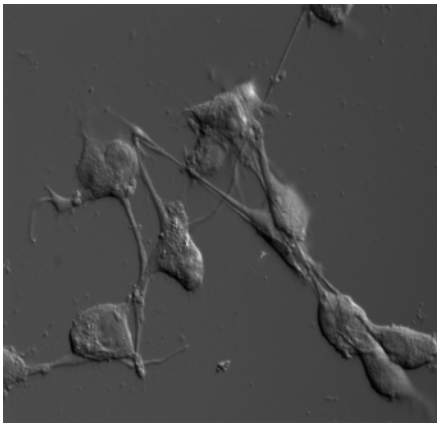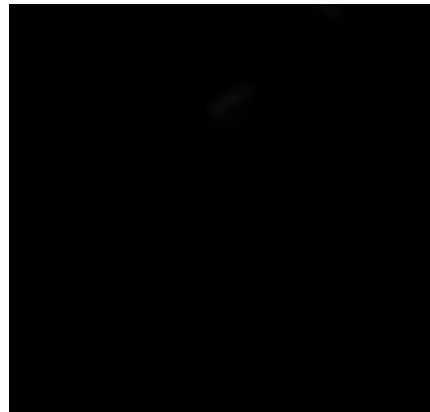
A
B

Figure 4.4: (A) DIC images and (B) Fluorescence images of cells that overexpress EGFr and have been directly labeled using goat anti-mouse IgG –Alexa 594
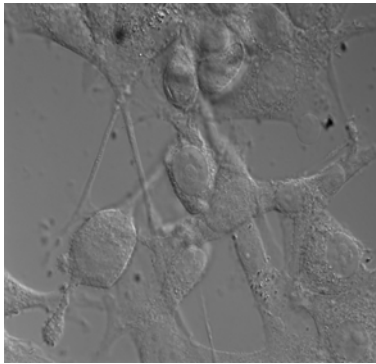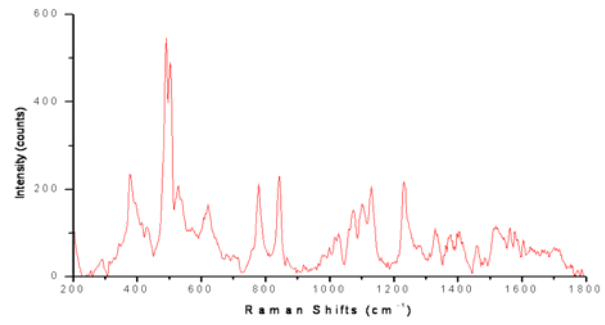
A   B

Figure 4.5: (A) DIC images and (B) SERS spectrum in cells overexpressing EGFr
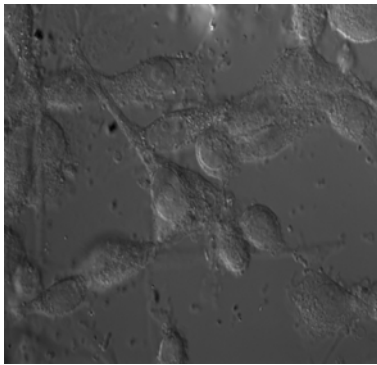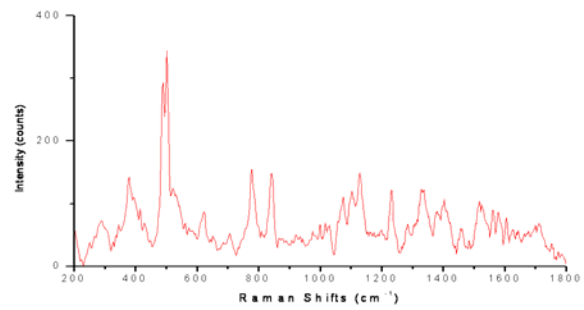
A   B

Figure 4.6: (A) DIC images and (B) SERS spectrum of in cells expressing normal levels of EGFr
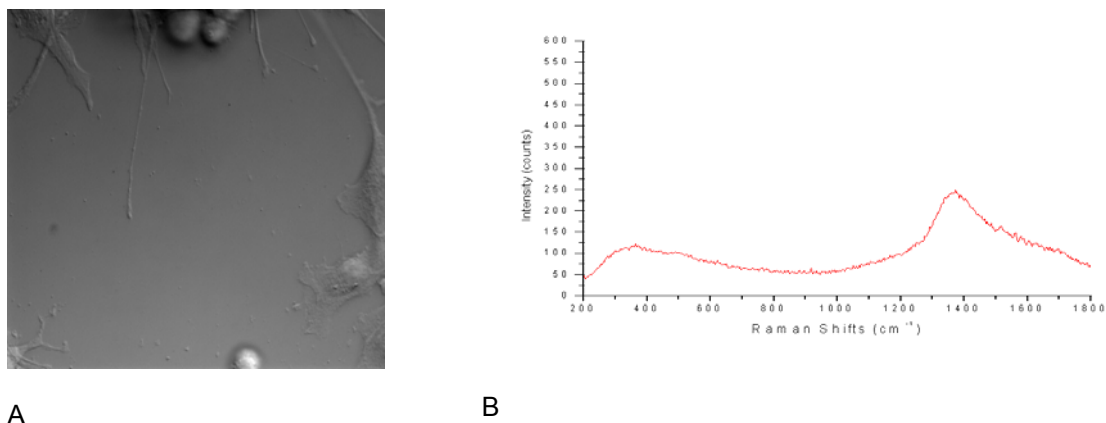
Figure 4.7: (A) DIC images and (B) SERS spectrum in the blank region of cells expressing normal levels of EGFr

4.3 Materials and Methods

4.3.1 Materials

U87 MG (Human glioblastoma-astocytoma) cells were obtained from the laboratory of Dr. Robert Bachoo, PhD, University of Texas Southwestern Medical Centre, Monoclonal mouse anti-human EGFR was obtained Dako and goat anti-mouse IgG Alexa Fluor 594 used as secondary was obtained from Invitrogen.

Other equipment and measuring devices are the same as used in chapter 3 above.

4.3.2 Method

The synthesized nanotags from chapter 3 were first purified by centrifugation at a g-force of 1000g for 15 min to remove excess SH-PEG-COOH. After purification, the nanotags were resuspended in Deionized water having a pH of 5.5. This purification is done three times. After this the nanotags are reacted with EDC (10 ul of 20 mg/ml) and Sulfo-NHS (10 ul of 55 mg/ml) for 600 ul nanotag solution (2.6 x 10^{13}particles/l). The reaction was done in room temperature for 15 minutes under rapid stirring of nanotag solution. The resulting solution was then purified again by 3 times of centrifugation under the same condition as before. In the final centrifugation the nanotags are resuspended in PBS. Some polyethylene glycol should be added to reduce loss of nanotags through sticking on the centrifuge tube walls. EGFr is was

added to the solution so that the EGFr added was 1:200 diluted. EGFr is reacted in the nanotag solution for 2 hours at room temperature then overnight at 4 ^{O}C. The functionalized nanotags are then purified by centrifugation and resuspended in PBS.

In the conjugation of the nanotags onto the cells, the normal procedure for immunocytochemitry. To begin with the cells were blocked using serum from the same animal as were the secondary is grown. In this case this was goat serum. 100 ul of serum was added to each well and then incubated in room temperature for one hour. Washing was done using PBS, three times for 15 minutes each time. After the washing, 100 ul of nanotag solution was added to the wells of interest and plain primary antibody is added some of the wells. The reaction is done for 2 hr at room temperature then overnight at 4 ^{o}C. The wells are then washed again, three times for 15 minutes each time using. 100 ul goat anti-mouse IgG-Alexa 594 was then added each well and then incubated for about one hour before 3 times wash.

The cells were then imaged using fluorescence microscope and The Raman system.

CHAPTER 5

CONCLUSION AND FUTURE WORK

5.1 <u>Conclusion</u>

Raman nanotags have been synthesized with the potential for multiple biomolecular detection. In the design of the nanotags it is found that the suitable gold nanoparticles that could be used are 60 -65 nm gold nanoparticles with citrate coating. Although, these provide the best signal of the nanoparticles synthesized it should be noted that the one step seed growing method described by Jian Niu allows for better control of size and shape of nanoparticle during synthesis.

The stability of the nanotags once coated with PEG coating, even under biological conditions gives them potential for use in biological environments. PEG seems provide an adequate enough coating to keep the nanoparticles dispersed and the dye adsorbed on the gold nanoparticles.

The ability to identify visual, multicolor nanotags in mixtures indicates suggests the possibility of developing a system based on software identification of nanotag peaks. This has the potential of allowing greater resolution and hence identification of even more nanotags within mixtures.

Functionalization of Raman nanotags and specific targeting of biomolecules using these functionalized nanotags is vital for the practical application of the nanotags. In the, thesis, it was possible to show that there is some indication of higher signal for tumor cells and lower signal for normal cells, however, there is need to improve on the signal to noise ratio inorder to allow for clear and quantitative discrimination between tumor and normal cells. The most likely cause of this reduced signal to noise ratio is low yield in functionalization of the nanotags.

37

5.2 <u>Future work</u>

Although the signal for SERS remains stable when a nonfluorescent dye is used, it varies from batch to batch. This presents a problem practical application for a quantitative approach requiring calibration for each batch. To overcome this, it is possible to tune SERS signal to a predermined value. Preliminary tests with DTTC Iodide indicate that this is possible within a given range.

Additionally, for biological application, the biodistribution of the nanotags is important information to acertain whether the nanotags are able to target tumor cells within a body and what   within   what   time   window   are   they   retained   at   the   tumor   site.

REFERENCES

1. Cheng C, Ming M, Cuda G, Bunimuvich Y L, Gspari M, Heath J R, Hill H D, Mirkin C A, Nijdam A J, Tarracciano R, Thundat T and Ferrari M. " Nanotechnologies for biomolecular detection and medical diagnostics." Curr. Opin. Chem. Biol. 10, 11–19 (2006).

2. Alarmo E L, Rauta J, Kauraniemi P, Karhu R, Kuukasjarvi T, Kallioniemi A, " Bone Morphogenetic protein 7 is widely overexpressed in Primary Breast Cancer," Genes, chromosomes & cancer 45, 411 – 419 (2006)

3. Meriaudeau F, Ferrell T L, Arkawa E T, Wig A, Passian A, Thundat T, Shen J, Patel S and Kraemer F B. "Study of different hormone-sensitive lipase concentrations using surface plasmon resonance sensor". Sensors and Actuators B: Chemical, 73, 192 – 198 (2001)

4. Sun L, Chenxu Y and Irudayaraj J.   "Surface-Enhanced Raman Scattering Based Nonfluorescent Probe for Multiplex DNA detection." Anal. Chem. 79, 3981-3988 (2007)

5. http://www.hivaidscare.com/hivtesting.php?acode=na

6. Loberg R D, Fridman Y, Peinta B A, Keller E T, McCauley L K, Taichman R S, and Pienta K J, " Detection and Isolation of circulating Tumor cells in urologic cancers: a review," Neooplasia 6, 303 – 309 (2004

7. Zaheer A, Lenkinski R E, Mahmood A, Jones A G, Cantley L C, Frangioni J V, "In vivo near-infrared fluorescence imaging of osteoblastic activity," Nat. Bio. 19, 1148 – 1154 (2001)

8. Jiang W. Martin T A, Mansel R E. "Molecular detection of micro-metastasis in breast cancer". Critical Reviews in Oncology/Hematology. 43, 13-31(2002)

9. Isola N. R. et al. Surface-Enhanced Raman Gene Probe for HIV Detection. Anal. Chem. 70, 1352-1356 (1998)

10. Ni J et al. Immunoassay Readout Method Using Extrinsic Raman Labels Adsorbed on Immunogold Colloids. Anal. Chem. 71, 4903-4908 (1999)

11. Fleischmann, M.; Hendra, P. J.; McQuillan, A. "Raman Spectra of Pyridine Adsorbed at a Silver Electrode" J. Chem. Phys. Lett., 26, 163-166, (1974)

12. Kneipp, J.; Kneipp, H.; Rice, W. L.; Kneipp, K. "Optical Probes for Biological Applications Based on Surface-Enhanced Raman Scattering from Indocyanine Green on Gold Nanoparticles" Anal. Chem., 77, 2381-2385, (2005)

13. Vo-Dinh, T." Surface-enhanced Raman spectroscopy using metallic nanostructures" Trends Anal. Chem. 17, 557-582, (1998)

14. A. M. Michaels, M. Nirmal and L. E. Brus "Surface Enhanced Raman Spectroscopy of Individual Rhodamine 6G Molecules on Large Ag Nanocrystals", J. Am. Chem. Soc., 121, 9932–9939, (1999)

15. A. M. Michaels, J. Jiang and L. Brus," Ag Nanocrystal Junctions as the Site for Surface-Enhanced Raman Scattering of Single Rhodamine 6G Molecules" J. Phys. Chem. B, 104,11965–11971, (2000)

16. K. A. Bosnick, J. Jiang and L. E. Brus," Fluctuations and Local Symmetry in Single-Molecule Rhodamine 6G Raman Scattering on Silver Nanocrystal Aggregates" J. Phys. Chem. B, 106, 8096–8099, (2002)

17. P. Etchegoin, H. Liem, R.C. Maher, L.F. Cohen, R.J.C. Brown, H. Hartigan, M.J.T. Milton, J.C. Gallop "A novel amplification mechanism for surface enhanced Raman scattering" Chemical Physics Letters, 366, 115–121, (2002)

18. E. J. Bjerneld, P. Johansson and M. Kall, " Single Molecule Vibrational Fine-structure of Tyrosine Adsorbed on Ag Nano-Crystals" Single Mol., 1,239–248, (2000)

19. H. X. Xu, J. Aizpurua, M. Kall and P. Apell, "Electromagnetic contributions to single-molecule sensitivity in surface-enhanced Raman scattering" Phys. Rev. E, 62, 4318–4324 (2000)

20. Jackson J B, Westcott S L, Hirsch L R, Halas N J, "Controlling the surface enhanced Raman effect via the nanoshell geometry "Appl. Phys. Lett., Vol. 82, No. 2, 13 (2003)

21. Kneipp, K.; Wang, Y.; Kneipp, H.; Perelman, L. T.; Itzkan, I.; Dasari, R. R.; Feld, M. S. "Single Molecule detection using Surface Enhanced Raman Spectroscopy" Phys. Rev. Lett. 78, 1667. (1997)

22. Nie, S. M.; Emory, S. R. "Probing Single Molecules and Single Nanoparticles by Surface-Enhanced Raman Scattering" Science, 275, 1102 (1997)

23. Ruan C, Wang W and Gu B, " Single-molecule detection of thionine on aggregated gold nanoparticles by surface enhanced Raman scattering," J. Raman Spectrosc. 38: 568–573 (2007)

24. Ni, J.; Lipert, R. J.; Dawson, G. B.; Porter, M. D. "Immunoassay Readout Method Using Extrinsic Raman Labels Adsorbed on Immunogold Colloids "Anal. Chem. 71, 4903-4908. (1999)

25. Mulvaney, S. P.; Musick, M. D.; Keating, C. D.; Natan, M. J. "Glass-Coated, Analyte-Tagged Nanoparticles: A New Tagging System Based on Detection with Surface-Enhanced Raman Scattering" Langmuir, 19, 4784-4790 (2003)

26. Ferraro J. R., Nakamoto K, Brown C W, "Introduction to Raman Spectroscopy, Second Edition", Academic Press, 6, (2003)

27. Anderson L. G. http://carbon.cudenver.edu/public/chemistry/classes/chem4538/raman.htm

28. Infotonics inc. www.medisciencetech.com/append/OpticalBiopsyPill.htm

29. Qian M. X, Nie S. M. "Single-molecule and single-particle SERS: from fundamental mechanisms to biomedical appliations." Chem. Soc. Rev., 37, 912–920 (2008)

30. Kim J, Kim J, Choi H, Lee S, Jun B, Yu K, Kum E, Kim Y, Jeong D H, Cho M and Lee Y, "Nanoparticle Probes with Surface Enhanced Raman Spectroscopic Tags for Cellular Cancer Targetting", Anal. Chem., 78, 6967-6973, (2006)

31. Qian X, Peng X, Ansari D O, Yin-Goen Q, Chen G Z, Shin D M, Yang L, Young A N, Wang M D, Nie S, "*In vivo* tumor targeting and spectroscopic detection with surface-enhanced Raman nanoparticle tags", Nat. Biotech. 26, 83 – 90, (2008)

32. Zaveleta C, de la Zerda A, Liu Z, Keren S, Cheng Z, Schipper M, Chen X, Dai H, Gambhir S, " Noninvasive Raman Spectroscopy in Living Mice for Evaluation of Tumor Targeting with Carbon Nanotubes." Nano Lett., 8 (9), 2800 – 2805 (2008)

33. Keren S, Zeveleta C, Cheng Z, de la Zerda A, Gheysens O, Gambhir S S, "Noninvasive molecular imaging of small living subjects using Raman Spectroscopy." PNAS, 105, 5844 – 5849, (2008)

34. Spruck M "Gold Therapy for Rheumatoid Arthritis," The American Journal of Nursing, 79, 1246 – 1248, (1979)

35. Connor, E.E., Mwamuka, J., Gole, A., Murphy, C.J. & Wyatt, M.D. Gold nanoparticles are taken up by human cells but do not cause acute cytotoxicity. Small 1, 325–327, (2005).

36. Shukla, R. et al. Biocompatibility of gold nanoparticles and their endocytotic fate inside the cellular compartment: a microscopic overview. Langmuir 21, 10644–10654, (2005).

37. Abraham G D, Himmel P B, "Management of Rheumatoid Arthritis: Rationale for the use of colloidal metallic gold," Journal of Nutritional & Environmental Medicine, 7, 295 – 305 (1997)

38. Emory S R, Haskins W E, Nie S, "Direct observation of size-dependent optical enhancement in single metal nanoparticles," J. Am Chem. Soc, 120, 8009 – 8010 (1998).

39. Gao, X., Cui, Y.Y., Levenson, R.M., Chung, L.W.K. & Nie, S.M. In vivo cancer targeting and imaging with semiconductor quantum dots. Nat. Biotechnol. 22, 969–976 (2004).

40. Liu, Z. et al. In vivo biodistribution and highly efficient tumour targeting of carbon nanotubes in mice. Nat. Nanotechnol. 2, 47–52 (2007).

41. Weissleder, R., Kelly, K., Sun, E.Y., Shtatland, T. & Josephson, L. Cell-specific targeting of nanoparticles by multivalent attachment of small molecules. Nat. Biotechnol. 23, 1418–1423 (2005).

42. Frens, G., "Controlled nucleation for the regulation of the particle size in monodisperse gold suspensions," *Nature: Phys. Sci*., 241, 20 (1973)

43. Basu S, Ghosh S K, Kundu S, Panigrahi S, Praharaj S, Pande S, Jana S, Pal T, " Biomolecule induced nanoparticle aggregation: Effect of particle size on interparticle coupling," *Journal of Colloid and Interface Science* 313 (2007) 724–734

44. Panigrahi S, Basu S, Praharaj S, Pande S, Jana S, Pal A, Ghosh S K, Pal T, "Synthesis and Size-Selective Catalysis by Supported Gold Nanoparticles: Study on Heterogeneous and Homogeneous Catalytic Process," *J. Phys. Chem. C*, 2007, 111, 4596-4605

45. Niu J, Zhu T, Liu Z, "One-step seed-mediated growth of 30–150 nm quasispherical gold nanoparticles with 2-mercaptosuccinic acid as a new reducing agent," *Nanotechnology*: 18 (2007) 325607

46. Herbst RS. "Review of epidermal growth factor receptor biology". *Int. J. Radiat. Oncol. Biol. Phys.* 59: 21–26 (2004)

47. Kuan C T, Wikstrand C J, Bigner D D. "EGF mutant receptor vIII as a molecular target in cancer therapy". *Endocr. Relat. Cancer,* **8**, 83–96 (2001)

48. Libermann T A, Nusbaum H R, Razoni N, Kris R, Lax I, Soreq H, Whittle N, Waterfield M D, Ullrich A, Schlessinger J, "Amplification, enhanced expression and possible rearrangement of EGF receptor gene in primary human brain tumors of glial origin." Nature, 313, 144-147 (1985)

BIOGRAPHICAL INFORMATION

James Nyagilo was born on the 24th January 1980 in Eldoret, Kenya. He completed his primary school and secondary school education in Aga Khan Primary school, Kisumu and Nairobi School, Nairobi respectively, both in Kenya. His bachelors degree was in BS Physics at the Jomo Kenyatta University of Agriculture and Technology, in Juja Kenya from where He graduated in 2005. He had an attachment at the Radiation Protection Laboratories as a Radiation Protection Intern for about fourteen months before performing a stint at Longhorn Publishers Ltd were he worked as an Assistant Physics Editor.

In fall 2007, James began his graduate studies in Biomedical Engineering at the University of Texas in Arlington under the Joint Program of Biomedical Engineering at the University of Texas in Arlington and University of Texas Southwestern Medical Centre at Dallas. James in currently involved in research to develop a biomolecular detection system using Surface Enhanced Raman Spectroscopy as a platform.